atmosphere

MDPI

Article

Assessment of Carbonaceous Aerosol Properties across an Urban Environment during the Cold Season

Julija Pauraite *, Vadimas Dudoitis and Steigvilė Byčenkienė

Center for Physical Sciences and Technology (FTMC), Saulėtekio Ave. 3, LT-10257 Vilnius, Lithuania
* Correspondence: julija.pauraite@ftmc.lt

Abstract: For air quality management it is becoming increasingly important to be able to assess the quantity and properties of biomass-burning-related aerosol. Due to different chemical compositions and morphologies, black carbon (BC) and brown carbon (BrC) demonstrate diverse optical properties as well as an impact on air quality. In this study, we analyzed the chemical composition and light-absorbing properties of carbonaceous aerosol at an urban background station during the residential heating season. In addition, BC and BrC levels were assessed in six different areas in the city characterized by different predominant domestic heating systems. Positive matrix factorization (PMF) and BrC attribution analysis revealed that BrC mainly consisted of biomass-burning-related organic aerosol (BBOA) (up to 95%). The mass absorption cross-section at 370 nm for BBOA factors varied between 1.41 m^2g^{-1} and 2.63 m^2g^{-1}. The study of six different areas in the city showed that the input of BrC to the total light absorption coefficient within the city varied between 33% and 70%. In addition, the worst air quality was present in areas with numerous old wooden houses with outdated heating systems where significantly increased BC and BrC levels were observed.

Keywords: aerosol chemical composition; urban environment; black carbon; brown carbon; biomass burning

Citation: Pauraite, J.; Dudoitis, V.; Byčenkienė, S. Assessment of Carbonaceous Aerosol Properties across an Urban Environment during the Cold Season. *Atmosphere* **2023**, *14*, 1054. https://doi.org/10.3390/atmos14071054

Academic Editors: Francesca Costabile and Beatrice Moroni

Received: 16 April 2023
Revised: 17 May 2023
Accepted: 16 June 2023
Published: 21 June 2023

1. Introduction

Approximately one-fifth of Europeans reside in regions that are polluted by at least one type of airborne pollutant, leading to 500,000 premature deaths per year in Europe due to fine particulate matter (PM) [1,2]. Eastern and central European countries are particularly affected by poor air quality [3–5]. In cities and nearby areas, carbonaceous aerosols (such as organic carbon (OC) and black carbon (BC)) are making a substantial contribution to aerosol concentration and are thought to be particularly detrimental to human health [6–8]. It has been acknowledged that the increased mass concentration of carbonaceous aerosol across Europe in winter is largely due to residential-heating-related biomass burning [9–12]. Studies conducted by Crippa et al. (2014) [13] and Daellenbach et al. (2017) [14] suggest that the contribution of biomass-burning-related organic aerosol (BBOA) to total organic aerosol (OA) concentrations in Europe ranges from 12% to 59%. Meanwhile, Becerril-Valle et al. (2017) [12] reported that up to 88% of the mass concentration of BC was attributed to biomass burning during winter.

The emissions from biomass burning for residential heating can vary greatly based on the type of technology used, the fuel, and how the appliance is operated (e.g., hot or cold start, or flaming or start-up) [15–17]. Generally, these studies found that small appliances and open fires had higher emission factors. Yet, the scale to which different residential heating systems influence local air quality remains unknown.

In recent years, portable equipment has enabled urban air quality assessment close to pollution sources (such as households and busy roads). Blanco-Donaldo et al. (2022) [18] investigated biomass-burning- and traffic-related BC levels while moving on busy roads

and found that the average BC mass concentration was 16.1 μg/m^3 mainly due to traffic-related BC (66%). A similar study by Nie et al. (2022) [19] found that road-traffic-related BC accounted for 74% of the total BC. Another study by Moreno et al. (2020) assessed particle number distribution and concentration in several different locations around the globe and found that the majority of airborne urban particles were <100 nm in size and were associated with traffic. Yet, these studies focused on measurements close to roads during daytime when vehicles are commonly the main polluters, and the importance of domestic biomass burning was not properly assessed. In our study, we investigated BC and BrC levels attributed to biomass burning in urban background stations and in six areas with different dominant types of residential heating technology. Our aim was to understand the impact of different biomass burning technologies on local air quality, which is crucial for the improvement of related regulations and, as a result, the improvement of air quality in urban environments.

2. Methods

2.1. Sampling Sites

The Center for Physical Science and Technology campus, where the measuring site is located, is situated 8 km away from the city center and is relatively distant from main traffic roads or large local pollution sources, making it an ideal urban background (Figure 1). Yet, several residential buildings are located in the vicinity, and thus some biomass-burning-related emissions for residential heating purposes were expected. The climate in Vilnius is continental. Measurements at this location were performed from 8 October to 12 November 2021.

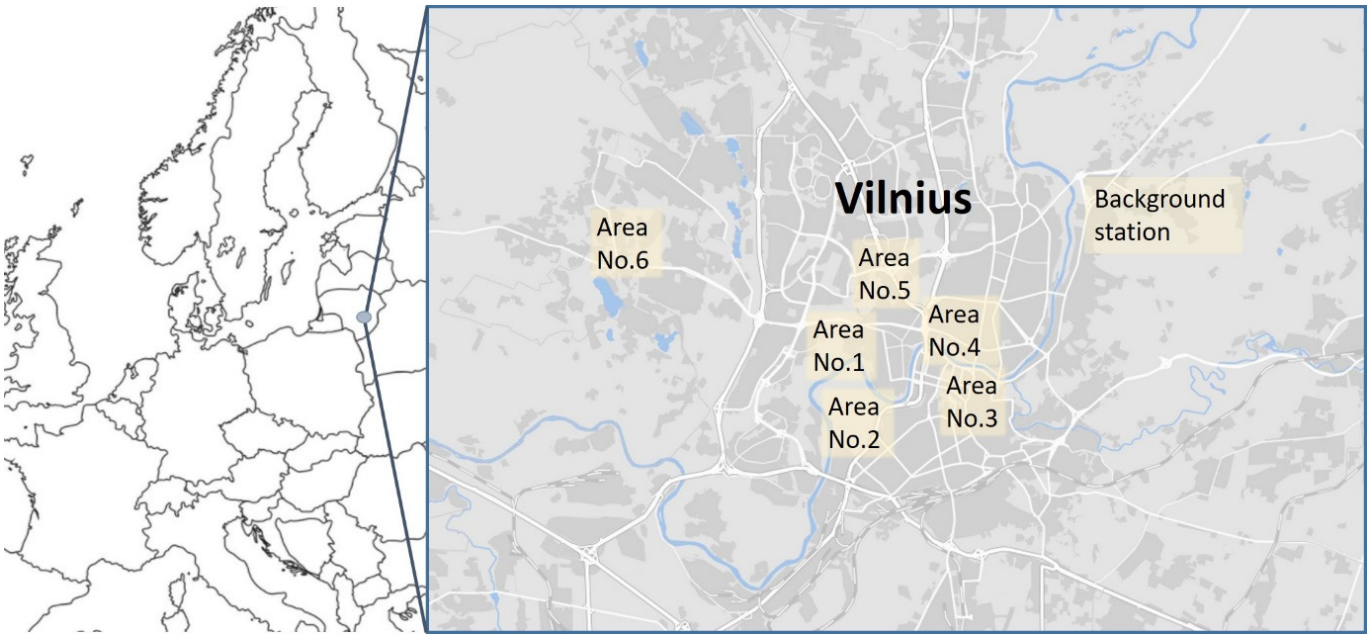

Figure 1. Map with sampling areas and background station.

Six different areas (Figure 1) were chosen because of their different dominant types of technology and fuel used for residential heating. Measurements at each location were performed for 3 h between 6 and 10 p.m. On all measurement days, no precipitation was present.

Area No. 1 is characterized by circa one-hundred-year-old wooden residential buildings. While many of these buildings are connected to the city's gas supply, numerous buildings are still using solid fuels such as wood. Due to a lack of regulations, most houses do not update their residential systems, and no exhaust filters are installed. Measurements

at this location were performed on 19 October 2021. During the measurements, several cars passed by. No traffic jams were observed.

Area No. 2 is characterized by the biggest city park (162 ha). The park contains an old forest, a botanical garden, and a river. While there are no local residential heating units in this area, it is located just next to Area No. 1, which is expected to be a high pollution source. Measurements at this location were performed on 23 October 2021. No traffic was present in the area. The park is only accessible to pedestrians.

Area No. 3 is better known as the old town of the city. Most of the buildings are historical brick-based houses with renovated domestic heating systems or connected to a centralized heating system. Yet, some old solid-fuel- and gas-based stoves remain. Measurements at this location were performed on 20 October 2021. Half of the old town is closed to traffic. In the remaining half, several vehicles passed by, but no traffic jams were observed.

Area No. 4 is the most diversified area. In this area, some of the buildings are modern offices, surrounded by several blocks of flats that are heated using a centralized system. Another part of the same area is covered by circa one-hundred-year-old wooden residential buildings using various heating methods. Measurements at this location were performed on 25 October 2021. Very few cars passed by in the vicinity.

Area No. 5 can be characterized as blocks of flats that are fully connected to the city's central heating system. No significant biomass burning source is located in this area. Most of the buildings were built in 1977–1980 and have not been modernized to this day. Measurements were performed on 11 November 2021. Very limited traffic was present in the area during measurements.

Area No. 6 is surrounded by newly-built (after the year 2000) individual houses. The central heating system is not available in this area. Yet, high-energy-class-related requirements were applied to most of the local buildings. Measurements were performed on 1 November 2021. During sampling, a few cars passed by. No traffic jams were observed.

2.2. Instrumentation

In the present study, BC and OA attributed to BrC were investigated, taking into consideration their different morphologies. Microscopy images show that freshly emitted BC particles are composed of hundreds of small spherical primary particles that have formed branched aggregates and are known for their significant light absorption properties across the entire ultraviolet (UV)-visible spectrum [20,21]. Meanwhile, the properties of BrC that can be quantified include a spherical shape in the aerosol mode and a strongly wavelength-dependent absorption spectrum that peaks in the UV spectral region and declines through the visible spectrum [20–22]. Thus, in this study, carbonaceous aerosols were attributed to BC and BrC based on differences in light absorption spectra.

Using an Aethalometer AE33 (Magee Scientific, Berkeley, CA, USA), light attenuation was measured with a quartz fiber filter 0.5 cm^2 in area and with a flow rate of 4 L min^{-1}. Each measurement was conducted every 5 min for 7 different wavelengths (370, 470, 520, 590, 660, 880, and 950 nm). For the evaluation of BC mass concentration, a standard MAC value was used (7.77 m^2/g) at 880 nm. The aethalometer was deployed at the background station, 10 m above ground level. For light absorption measurements in six different areas of the city, the portable Aethalometer Microaeth MA200 was used. Measurements were conducted with 1 min time resolution for 5 different wavelengths (375, 470, 528, 625, and 880 nm). For both aethalometers, AE33 and Microaeth MA200, sampling corrections were applied following Drinovec et al. (2015) [23].

The 'Aethalometer model' developed by Sandradewi et al. (2008) [24] was applied to assign BC to fossil fuels and biomass burning origin. For this aim, absorption Angström exponent (AAE) values of 0.9 for BC_{FF} and 1.68 for BC_{BB} were used following Zotter et al. (2017) [25]. The evaluation of light absorption by brown carbon ($b_{abs\ BrC}$) was performed based on the wavelength dependence method introduced by Qin et al. (2018) [26].

For the assessment of BrC chemical composition at the background station, an aerosol chemical speciation monitor (ACSM) was used. An ACSM measures the mass spectra and main chemical species of submicron aerosol particles with a time resolution of 30 min. The instrument measured aerosol particles ranging in size from 30 nm to 1 µm diameter while keeping relative humidity below 50%. Sampled submicron particles were focused onto a heated surface (600 °C), where the PM_1 components were vaporized. A 70 eV electron impact quadrupole mass spectrometer was used to detect and chemically characterize typical aerosol loadings (several $\mu g/m^3$). The ACSM provides mass spectra signals from *m/z* 12 to *m/z* 149. Following Middlebrook et al. (2012) [27], the collection efficiency (CE) was calculated. A positive mass factorization (PMF) [28] was performed for further analysis of organic aerosol mass spectra. PMF was applied to assign organic aerosol (OA) to different sources. This statistical tool converts the mass spectra of OA into a linear combination of several factor profiles, separating several time series and their associated mass. For PMF analysis, the multi-linear engine (ME-2) algorithm and SoFi 6.6 software were used. In addition, in order to reduce noisy signals, only signals up to *m/z* 120 were used for analysis. All PMF analysis was performed following the guidelines established by Paglione et al. (2020) [9]. OA factors from PMF solution were used for the assessment of BrC chemical composition. In order to understand which OA could be associated with BrC, the mass absorption cross-section (MAC) values of each OA factor were evaluated following Qin et al.'s (2018) [24] method consisting of a linear equation:

$$b_{abs\ BrC} = m_1 \times [OA_1] + m_2 \times [OA_2] + m_3 \times [OA_3] + m_4 \times [OA_4] + m_5 \times [OA_5], \quad (1)$$

Here $[OA_n]$ is the mass concentration of each OA factor from the PMF solution; and m_n is the corresponding MAC value established while solving the linear equation.

3. Results

3.1. Submicron Aerosol Chemical Composition at the Background Station

3.1.1. OA Source Apportionment

The source apportionment of submicron OA allowed the identification of one secondary OA (more oxidized OA (OOA)) and four different primary OA factors: hydrocarbon-like OA (HOA), two different biomass-burning OAs (BBOA1 and BBOA2), and local unknown OA (LOA) (Figure 2).

The profile of HOA is characterized by peaks of aliphatic hydrocarbons including *m/z* 41, 43, 55, 57, 69, 71, etc. The diurnal trend of HOA showed a very sharp increase in mass concentration during morning rush hours (at 7 a.m., the mean mass concentration reached 1.39 $\mu g/m^3$). Meanwhile, the evening peak was delayed and much lower (at 9 p.m., it reached 0.95 $\mu g/m^3$) due to the influence of atmospheric mixing height. The time series of HOA strongly correlated with BC mass concentration (r = 0.71) and with its part attributed to fossil fuels (BC_{FF}) (r = 0.61) (Figure 2). The average contribution of HOA to total OA (the sum of all OA factors) was 11% and was significant to total PM_1 (the sum of OA factors, secondary inorganics, and BC) (7%) (Figure 3).

Two different BBOA factors were identified without external constraints. Both spectra were stable and exhibited characteristic peaks at *m/z* 29 (CHO^+) and 60 ($C_2H_4O_2^+$), which are known to be fragments of wood burning marker levoglucosan [29]. Both BBOA factors had similar significant input to total OA (BBOA1, 25%, and BBOA2, 26%) and PM_1 mass concentration (both 16% (Figure 3)). The difference between these two factors appeared while analyzing diurnal trends and correlations with external time series. BBOA1 showed a slight increase in mass concentration during nighttime and reached the highest concentration at 9 p.m. (2.05 $\mu g/m^3$). The time series of BBOA1 showed a moderate negative correlation with wind direction (r = −0.51), which indicates that BBOA1 consists of locally emitted primary particles. In addition, it showed moderate correlations with $b_{abs\ BrC}$ (r = 0.64) and BC_{BB} (r = 0.64). Meanwhile, BBOA2 exhibited a characteristic diurnal trend with a midday minimum (0.97 $\mu g/m^3$ at 4 p.m.) and a high peak during evening hours (up to 2.67 $\mu g/m^3$ at 8 p.m.). Furthermore, its time series strongly correlated with

m/z 60 (r = 0.77), BC (r = 0.75), $b_{abs\ BrC}$ (r = 0.83), and BC_{BB} (r = 0.84). None of these biomass-burning-related OA factors could be associated with one specific wind direction, but pollution rose analysis (Figure S1) revealed that higher mass concentrations were rather associated with the northern and south-eastern directions. Both BBOA1 and BBOA2 factors were found to be associated with fresh biomass burning processes (Figure 4b) and this finding is in agreement with a triangle plot (Figure 4a). The triangle plot indicated that both BBOA1 and BBOA2 consisted of particles with no advanced atmospheric aging processes. While both BBOA1 and BBOA2 factors are associated with biomass burning from domestic heating, additional analysis is required to understand their different origins.

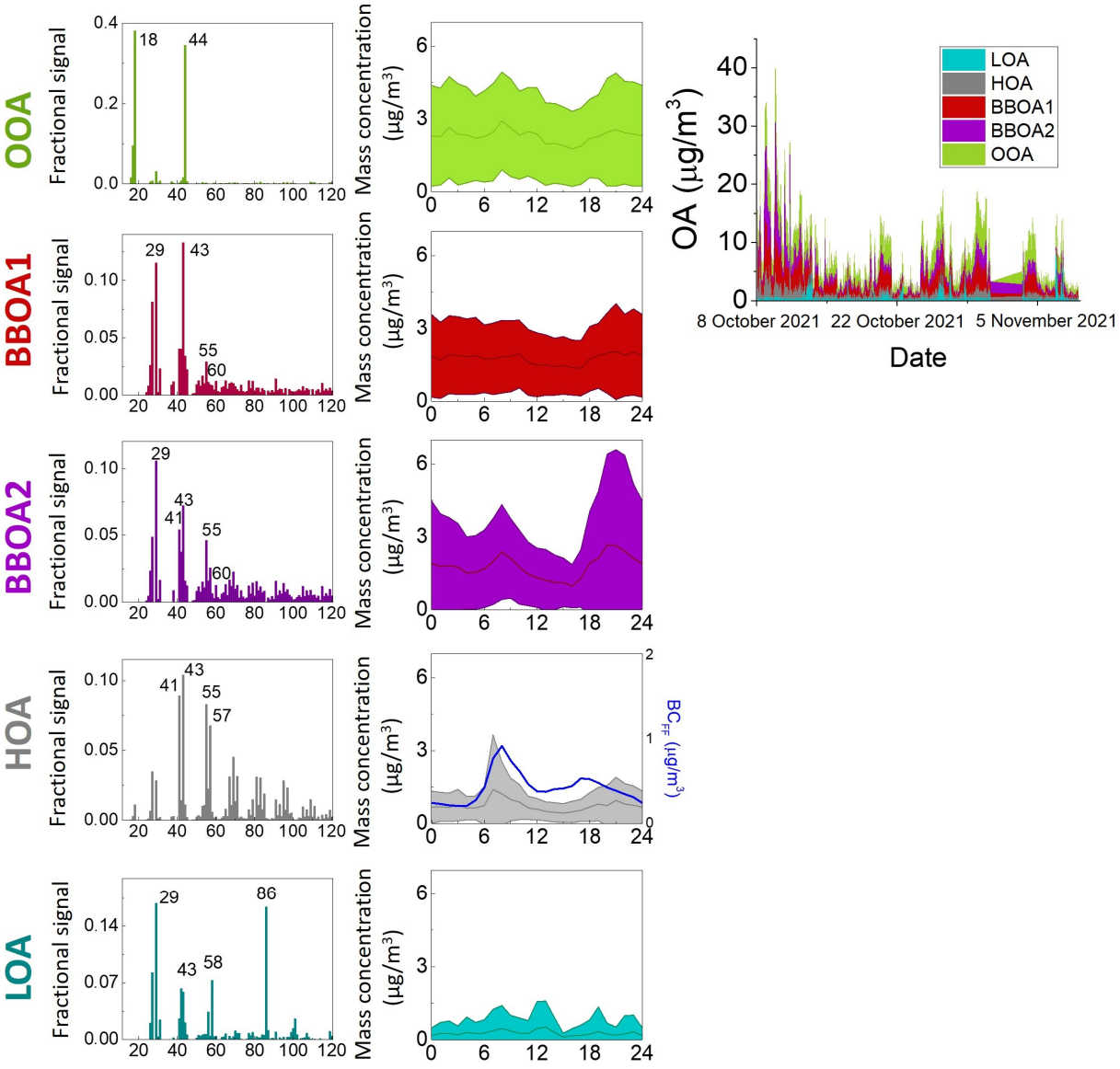

Figure 2. Mass spectra and diurnal trends of OOA (green), BBOA1 (dark red), BBOA2 (purple), HOA (grey), and LOA (light blue). In time series plots, the darker line represents the average, while the colored area shows the range of standard deviation. On the right—time series of OA mass concentration.

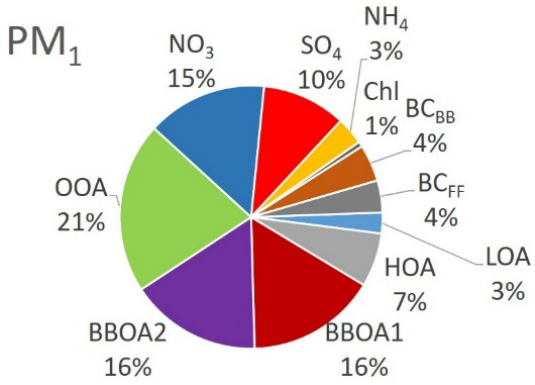

Figure 3. Pie chart of average PM_1 contributors at the background station.

Secondary OA factor OOA had a characteristic peak at m/z 44 (CO_2^+), which corresponds to the increased oxygenated fragments of the mass spectra. This factor was significantly more oxidized than the rest of the OA factors (Figure 4a) and was associated with background aerosol. The diurnal trend did not show a significant pattern, which is common for background OA. OOA showed the highest contribution to OA and PM_1 mass concentrations (34% and 21%, respectively) (Figure 3). In addition, biomass burning processes did not influence the OOA factor (Figure 4b).

The last OA factor was primary LOA. This factor was very stable and appeared in the PMF solution without any constraints. It showed no clear diurnal pattern and only sharp peaks (up to 7.9 μg/m^3) were observed in the time series. Peaks of LOA mass concentration were observed during daytime and were present for around two hours each. LOA contributed 4% to the total OA mass concentration and 1% to the total PM_1. The highest signals from the factor profile (m/z 29, 43, 58, and 86) did not match any other LOAs observed in previous studies of OA in Vilnius [30–32]. The LOA factor could be characterized as not atmospherically aged and with no biomass burning influence (Figure 4a,b). Pollution rose analysis (Figure S1) showed that the OA particles of the LOA factor were associated with the west and south-west wind directions, indicating emissions from one area of the city. In order to understand their origin, additional analysis closer to the source is required.

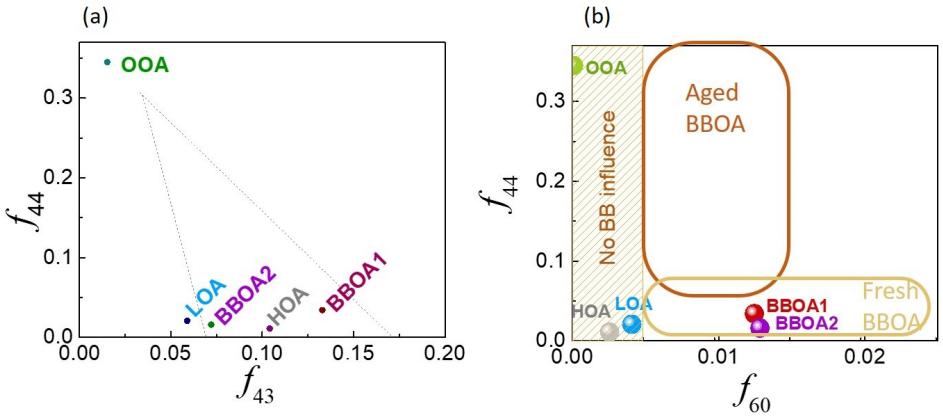

Figure 4. Triangle plot based on Ng et al. (2010) [33] (**a**) and f_{44} versus f_{60} space with associations with biomass burning (BB) influence, following Paglione et al. (2020) [9] (**b**).

3.1.2. BC and b_{abs} Source Apportionment

During the measurement campaign, the average BC mass concentration was 0.93 μg/m^3 (SD = 0.88 μg/m^3). BC mass concentration was attributed to BC_{FF} and BC_{BB} (Figure 5a). The contribution of BC_{BB} to the total BC mass concentration was slightly higher, by 54%, than that of BC_{FF} (46%) (Figure 5b). Meanwhile, their contribution to the total PM_1 on

average was 4% each (Figure 3). BC_{BB} had an average mass concentration of 0.5 μg/m^3 (SD = 0.6 μg/m^3). Its diurnal trend was characterized by a significant increase (on average 0.8 μg/m^3) during evening hours (around 8 p.m.) (Figure 5c). Additionally, the diurnal trend of BC_{BB} strongly resembled that of BBOA2. Besides the strong correlation with BBOA2 (r = 0.84), BC_{BB} also had a strong correlation with the time series of m/z 60 (r = 0.84) and a moderate correlation with BBOA1 (r = 0.64). Furthermore, the average mass concentration of BC_{FF} was 0.4 μg/m^3 (SD = 0.4 μg/m^3). A significant increase was observed in its diurnal trend during morning hours (between 7 and 8 a.m.), with BC_{FF} increasing up to 0.9 μg/m^3 on average (Figure 5d). This morning-rush-hour-related peak was consistent with the one observed in the HOA diurnal trend. Moreover, a moderate correlation between BC_{FF} and HOA was observed (r = 0.61). Thus, there was strong agreement between BC species and OA factors, and a strong influence of BB processes was observed in both BC and OA source apportionment.

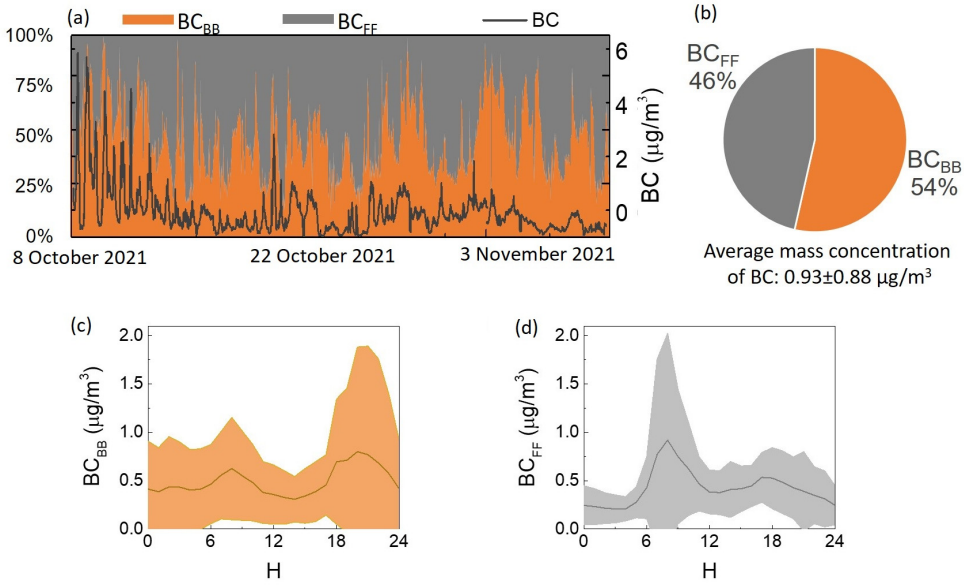

Figure 5. Time series of BC mass concentration and the relative contributions of BC_{BB} and BC_{FF} (**a**). Pie chart of BC_{FF} and BC_{BB} (**b**). Diurnal trends of BC_{BB} (**c**) and BC_{FF} (**d**).

Both BC_{BB} and BC_{FF}, together with BrC, contribute to the light absorption coefficient b_{abs}. b_{abs} light absorption spectra with the contributions of BC_{BB}, BC_{FF}, and BrC are depicted in Figure 6a,b. As can be seen in Figure 6a,b, BC_{BB} had the highest contribution to b_{abs} out of all b_{abs} spectra. The contribution of BC_{BB} varied between 62% (at 660 nm) and 50% (at 950 nm). $b_{abs\ BB}$ at 370 nm on average was 18.2 Mm^{-1} (SD = 19.7 Mm^{-1}). While the light absorption coefficient attributed to BC_{FF} ($b_{abs\ FF}$) reached its highest value at 370 nm (7.6 Mm^{-1}, SD = 7.8 Mm^{-1}), its contribution to the total b_{abs} at 370 nm was the lowest (24%) and increased up to 50% at 950 nm. Light absorption by BrC steadily decreased from 370 nm (7.2 Mm^{-1}, 22%) to 660 nm (0.7 Mm^{-1}, 6%). Light absorption by BrC at wavelengths higher than 880 nm is known to be not significant. Due to its highest importance, b_{abs} at 370 nm ($b_{abs\ 370}$) is investigated further in this study. On average, $b_{abs\ 370}$ was 33.2 Mm^{-1} (SD = 31.9 Mm^{-1}) but during the first week of the measurement campaign, it reached its highest value of 283.0 Mm^{-1} (Figure 6c).

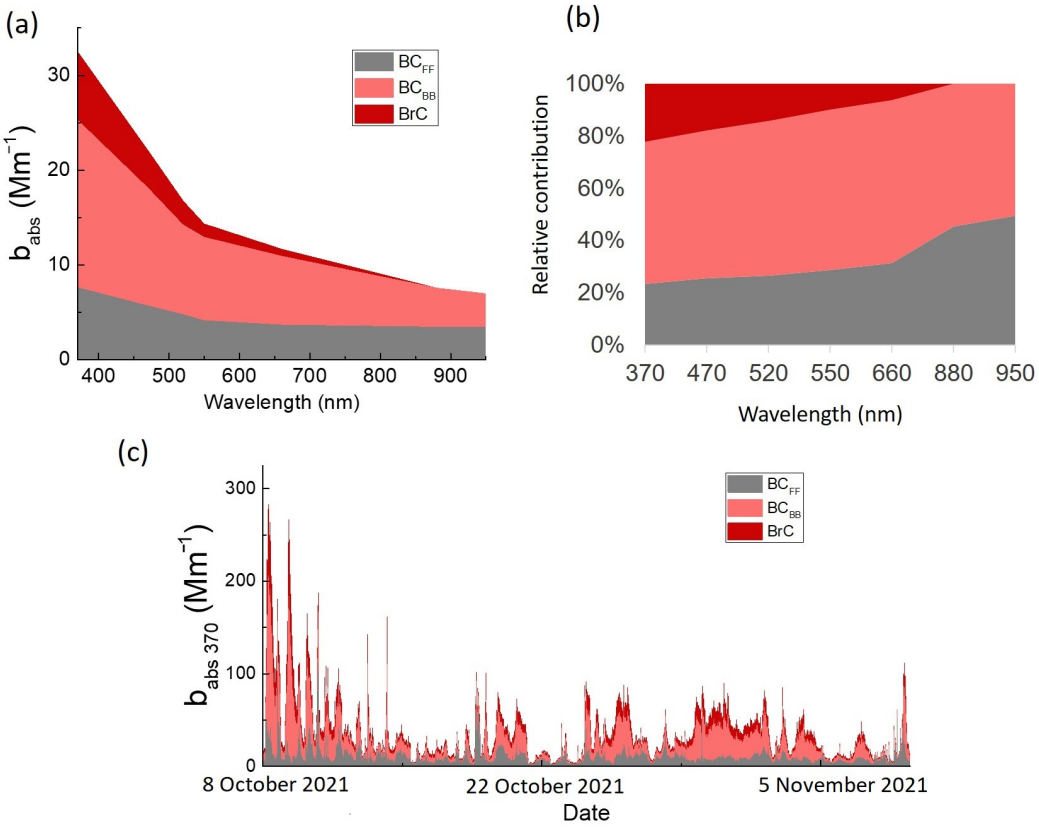

Figure 6. b_{abs} spectra together with its attribution to BC_{BB}, BC_{FF}, and BrC (**a**). Relative contributions for each carbonaceous species between 370 and 950 nm (**b**). Time series of b_{abs} (**c**).

3.2. BrC Sources and Optical Properties

Not all OA factors have light absorption properties. In this work, sources of $b_{abs\ BrC}$ at 370 were investigated, and light-absorbing OA factors were identified. Three OA factors showed non-zero mass absorption cross-section (MAC) values: BBOA1, BBOA2, and HOA (Figure 7a,b). The highest MAC value was estimated for BBOA2, which at 370 nm reached 2.63 m^2g^{-1}. This value steadily decreased to 0.23 m^2g^{-1} at 660 nm. Slightly lower MAC values were assigned to BBOA1, which varied between 1.41 m^2g^{-1} (at 370 nm) and 0.13 m^2g^{-1} (at 660 nm). Meanwhile, the MAC value estimated for HOA was the lowest. It remained rather stable between 370 nm and 470 nm (on average 0.59 m^2g^{-1}) and then gradually decreased to 0.04 m^2g^{-1} at 660 nm.

BBOA2 and BBOA1 contributed the most to $b_{abs\ BrC}$ at 370 nm (62% and 33%, respectively) (Figure 7c,d). Only 5% of $b_{abs\ BrC}$ at 370 nm was attributed to HOA. This shows the significant importance of biomass burning processes to light absorption by BrC. Additionally, the relative contribution of the $b_{abs\ BrC}$ plot (Figure 7d) shows that the contribution of HOA varied in a narrow range with a standard deviation of 9.9%. This allows us to conclude that the importance of HOA to $b_{abs\ BrC}$ is rather limited. The $b_{abs\ BrC}$ diurnal cycle for the duration of the measurement campaign (Figure 7e) indicates that the highest values of $b_{abs\ BrC}$ were observed during nighttime. Furthermore, the relationship between $b_{abs\ BrC}$ and levoglucosan-related peaks (m/z 29 and 60) was assessed. Figure 8a depicts m/z 29 versus m/z 60 space where $b_{abs\ BrC}$ is plotted in a color-coded scheme. As can be seen, $b_{abs\ BrC}$ increases with both m/z 29 and 60 higher intensities. While no significant correlation was observed between $b_{abs\ BrC}$ and m/z 29, a very strong correlation was found between $b_{abs\ BrC}$ and m/z 60 (r = 0.82). In view of this, we can conclude that $b_{abs\ BrC}$ is dominated by biomass-burning-related OA.

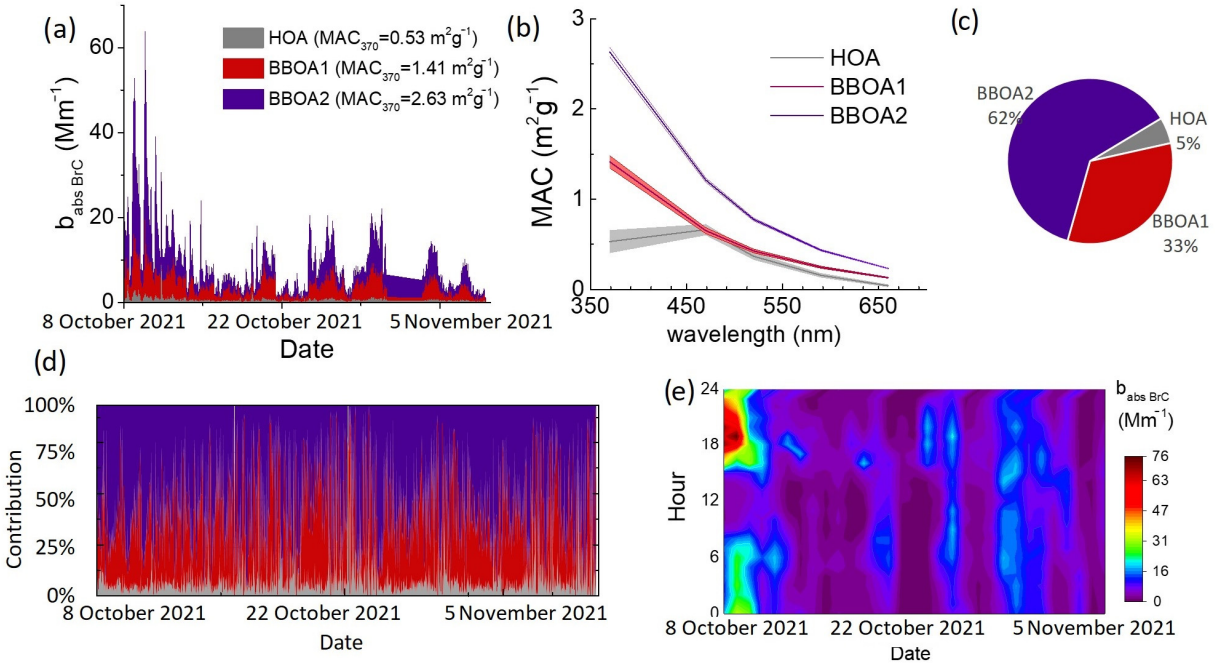

Figure 7. Time series of $b_{abs\ BrC}$ with each contributor (HOA, BBOA1, and BBOA2) (**a**). The spectrum of MAC values for HOA, BBOA1, and BBOA2 (**b**). Pie chart with average contributions of HOA, BBOA1, and BBOA2 at 370 nm (**c**). Time series of the relative contributions of HOA, BBOA1, and BBOA2 to $b_{abs\ BrC}$ (**d**). Spectral variation of $b_{abs\ BrC}$ during all measurement campaigns (**e**).

Besides the evident link between BB-related OA and BrC, a connection between BrC and meteorological parameters was observed. A strong negative correlation was observed between daily averages of $b_{abs\ BrC}$ and relative humidity (RH) ($r = -0.76$) (Figure 8b). This negative correlation suggests that with increased RH, scavenging processes are activated, resulting in decreased mass concentration of hydroscopic aerosol. Thus, OA contributing to BrC is likely to be hydroscopic. Additionally, due to possible delays between increased RH and efficient scavenging processes, no significant correlation was observed for raw (not averaged) data, but it appeared for daily averaged data points. Furthermore, a link between BrC and wind speed (WS) was observed. A moderate negative correlation ($r = -0.45$ for not-averaged data and $r = -0.54$ for daily averages) indicates that BrC particles were mostly emitted in the city. Therefore, with lower wind speed, particles are not well spread through space and are rather accumulating.

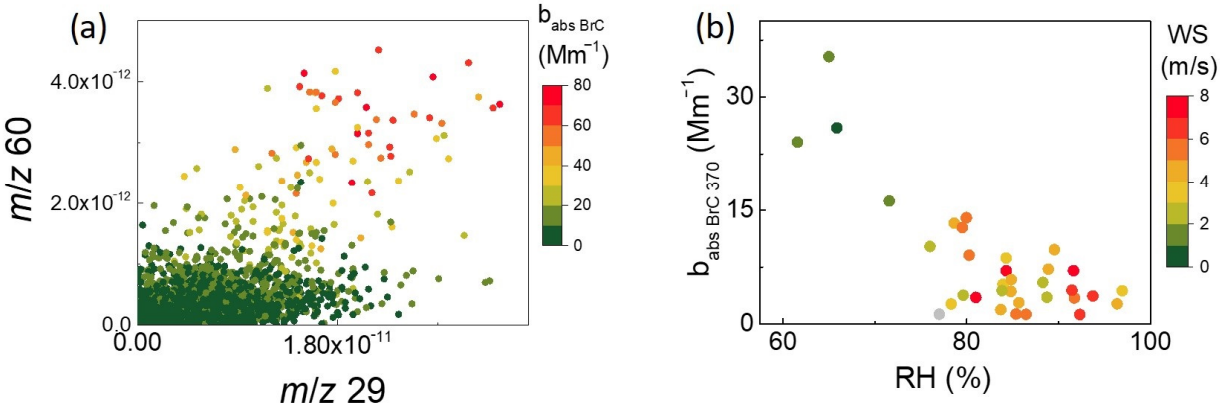

Figure 8. m/z 29 versus m/z 60 space together with $b_{abs\ BrC}$ (color-coded) (**a**). The relationship between $b_{abs\ BrC}$ and meteorological parameters: RH (x-axis) and WS (color code) (**b**). The data points in plot b are daily averages.

While biomass-burning- and traffic-related emissions are sources of BrC, they are also known sources of BC. Figure 9 depicts BC versus BrC space, where HOA and BB-related OA are used as proxies for traffic and biomass burning particle emissions. As can be seen in Figure 9, while BB processes are similarly important for both BrC and BC particle emissions, traffic-related aerosols contribute significantly more to BC than to BrC.

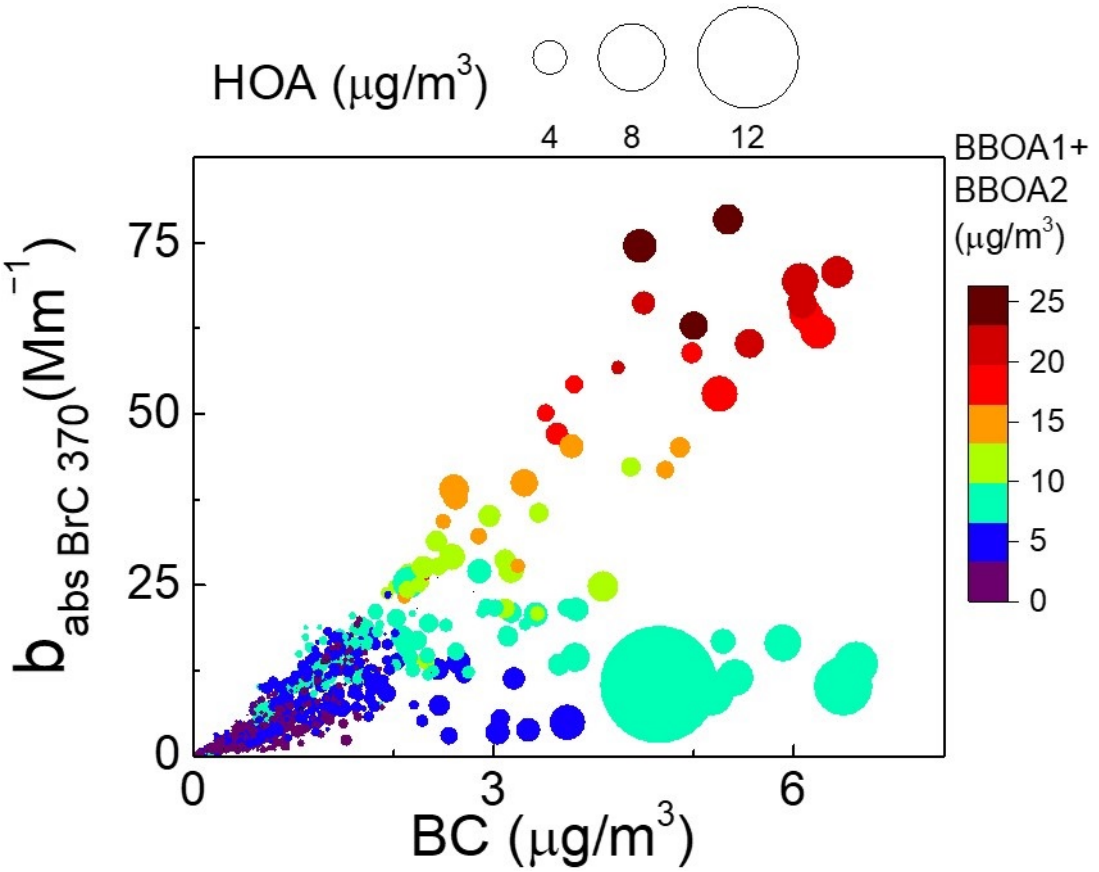

Figure 9. BC mass concentration versus $b_{abs\ BrC}$ intensity together with HOA and BB-related OA as size and color functions, respectively.

3.3. Comparison of Carbonaceous Aerosol between Different Areas of the City

After analyzing carbonaceous aerosol at the background station, the results were compared with those from six different areas of the city. b_{abs} spectra with attribution to BC_{BB}, BC_{FF}, and BrC were plotted for each area (Figure 10). The highest b_{abs} values (max 336.8 Mm^{-1}, and 188.7 Mm^{-1} on average, at 375 nm) were observed in Area No. 1, which is characterized by 100-year-old wooden buildings using various domestic heating fuels (wood, gas, and others). It was dominated by the contribution of BC_{BB} (60%), while the contribution of BrC reached 24%. In another area (Area No. 4) with many diversified buildings including old wooden houses, lower b_{abs} values were observed (on average 103.8 Mm^{-1} at 375 nm). In this area, the contributions of BC_{BB} (61%) and BrC (27%) were close to those observed in Area No. 1. Similar values of b_{abs} and its dominant contributions were found in Area No. 6 (on average 102.7 Mm^{-1} at 375 nm; contribution of BC_{BB} of 58% and BrC, 25%). In contrast to the previously mentioned areas, Area No. 6 is characterized by newly constructed individual houses. b_{abs} in Areas No. 3 and 5 were lower (83.9 Mm^{-1} and 71.8 Mm^{-1} at 375 nm, respectively) but BC_{BB} remained the dominant contributor (58% and 59%, respectively). The lowest b_{abs} values (on average 34.4 Mm^{-1} at 375 nm) were observed in Area No. 2, which is characterized as the biggest park in the city. In this area, the contribution of BC_{BB} became dominant only at 880 nm (97%) while the BrC contribution

varied between 39% (at 375 nm) and 44% (at 528 nm). Within longer wavelengths, the importance of BC_{BB} was increasing in all six areas.

In order to compare different areas of the city, additional assessment is required. Since all six areas were measured on different dates, all the time series were compared to those from the background station. As can be seen in Figure 11, b_{abs} (at 370 nm) levels were always lower at the background station than in the selected areas. The biggest difference was observed in Area No. 2 where $b_{abs\ BrC}$ was 10.7 times higher than at the background station. In addition, $b_{abs\ BB}$ was 8.0 times higher. Yet, during the sampling period in Area No. 2, most of the values were close to the measuring limit, which likely had an influence on the results. In Area No. 1, b_{abs} attributed to BrC and BC_{BB} were, respectively, 4.6 and 4.4 times higher than those at the background station. Similar results were observed in Area No. 4, where b_{abs} attributed to BrC and BC_{BB} were 4.0 and 3.8 times higher, respectively. Meanwhile, in another area characterized as containing old buildings (Area No. 3), $b_{abs\ BrC}$ and $b_{abs\ BB}$ were up to 2.5 times higher than at the background station. These results indicate that residential heating in old wooden houses has a significant impact on air quality locally and in neighboring areas.

Significantly lower differences between local b_{abs} and the ones at the background station were found in Areas No. 5 and 6. In Area No. 6, both $b_{abs\ BrC}$ and $b_{abs\ BB}$ were 1.8 higher compared to those at the background station. Meanwhile, the lowest difference was found in Area No. 5, which is characterized by blocks of flats using a central heating system. In this area, $b_{abs\ BrC}$ and $b_{abs\ BB}$ were 1.6 times higher than at the background station. In view of this, we can conclude that while residential heating systems in newly constructed buildings emit less pollution, the lowest pollution levels were found in areas with predominance of centralized heating systems.

In addition to residential-heating-related $b_{abs\ BB}$ and $b_{abs\ BrC}$, traffic-related $b_{abs\ FF}$ was compared within different areas. In Areas No. 1, 2, 4, and 6, $b_{abs\ FF}$ was between 2.8 and 3.0 times higher than $b_{abs\ FF}$ at the background station. Slightly smaller differences were found in Area No. 5 (2.1 times higher). Thus, in urban areas, traffic-related pollution rates were 2 to 3 times higher than at the background station.

Finally, BC levels (at 880 nm) were assessed in different locations. Only in Areas No. 2 and 5 were BC levels similar (0.8 and 1.3 times higher) to those at the background station. A slightly higher BC mass concentration compared to the background station was found in Area No. 6 (1.6 times higher). In the remaining areas (No. 1, 3, and 4), which all contain old buildings, BC levels were 2–3 times higher than the BC level measured at the background station (2.9, 1.9, and 2.2, respectively). Thus, the air quality in areas with older buildings was poorer due to increased BC mass concentrations.

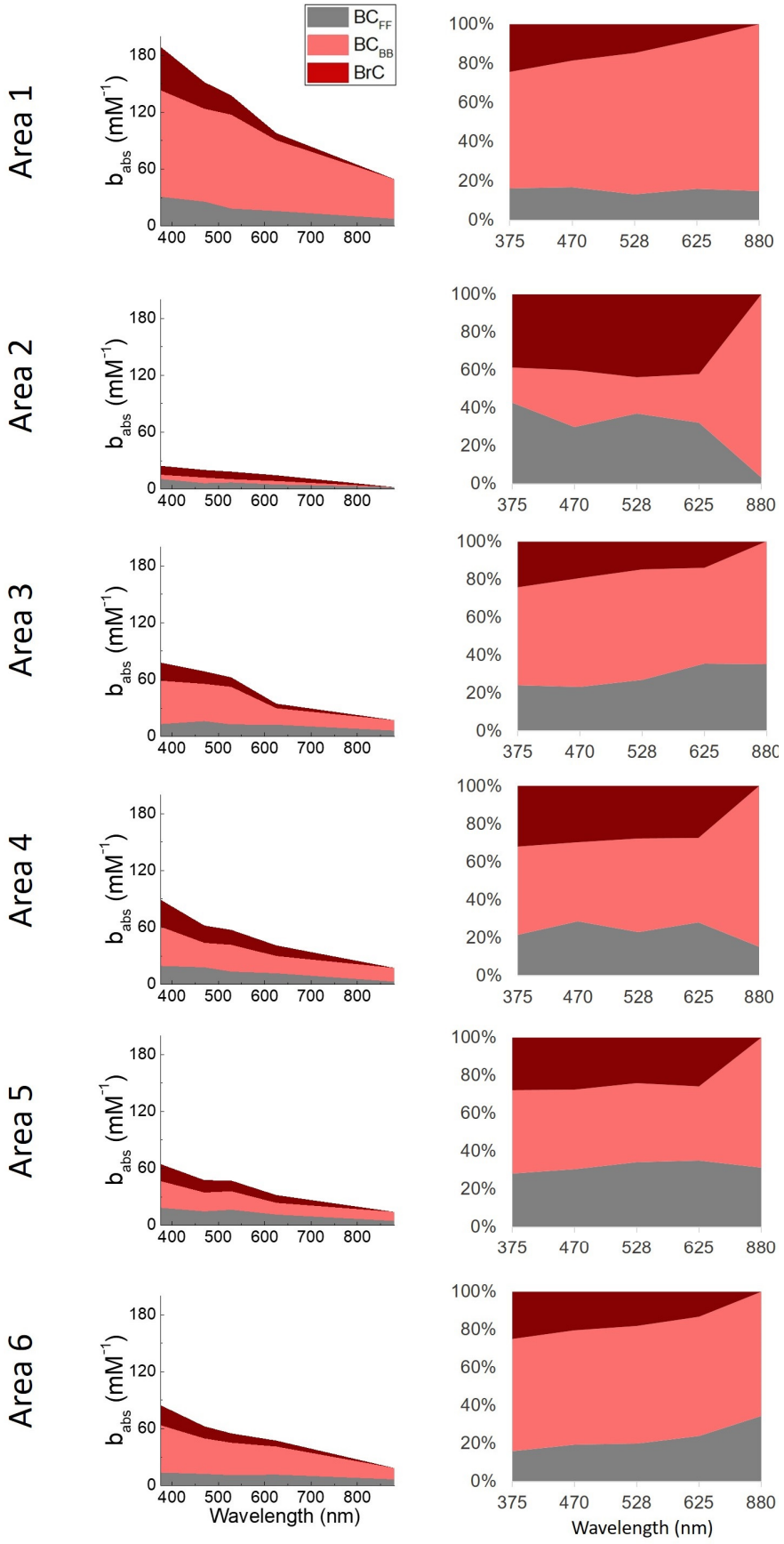

Figure 10. b_{abs} spectra in each area with contributions and relative contributions of BrC, BC_{BB}, and BC_{FF}.

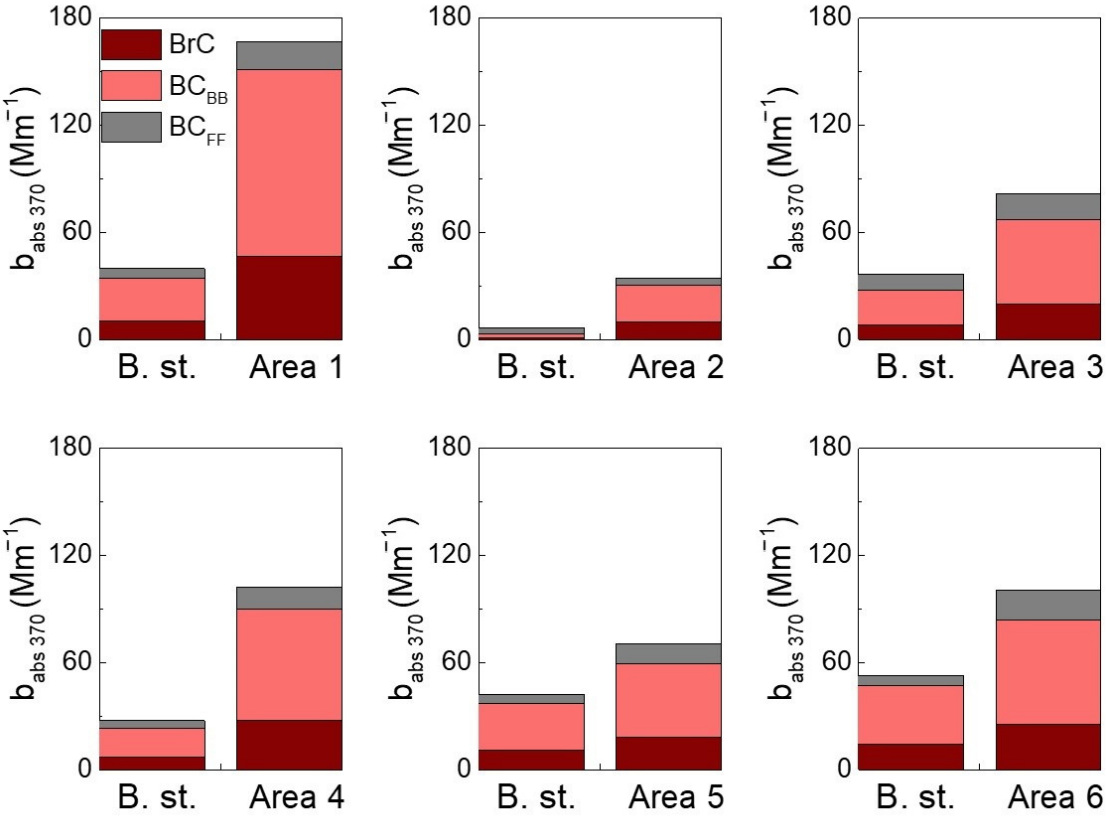

Figure 11. Stacked column graphs of $b_{abs\ 370}$ with its contributors in each area and at the background station (B. st.) during the same measurement period.

For the further assessment of each characteristic area of urban background, the delta of $b_{abs\ BrC}$ ($\Delta b_{abs\ BrC} = b_{abs\ BrC}(area) - b_{abs\ BrC}(background\ station)$) and delta of BC ($\Delta BC = BC(area) - BC\ (background\ st.)$) were calculated. In addition, all results were depicted in $\Delta b_{abs\ BrC}$ versus ΔBC space (Figure 12). As can be seen in Figure 12, the highest values of both $\Delta b_{abs\ BrC}$ and ΔBC were observed in Area No. 1, which is characterized by 100-year-old wooden houses using various heating methods. In addition, another area with higher $\Delta b_{abs\ BrC}$ and ΔBC values was Area No.4, which contains old wooden buildings as well. This indicates that areas with non-modernized residential heating systems suffer from lower air quality. Values of $\Delta b_{abs\ BrC}$ and ΔBC were similar in Areas No. 3 and 6. Buildings in Area No. 3 are historically old, yet most of them have been renovated, resulting in lower pollution levels and making local emissions similar to those of newly constructed houses in Area No. 6. While ΔBC was the lowest in the largest park in the city (Area No. 2), there was still an evident higher $b_{abs\ BrC}$ level due to highly polluted areas in close vicinity (such as Area No. 1). Yet, it is important to have in mind that during measurements in Area No. 2, the mass concentration of airborne particles was abnormally low. Meanwhile, in Area No. 5, which is characterized by centrally heated blocks of flats, both $\Delta b_{abs\ BrC}$ and ΔBC were very low. This allows us to conclude that centralized heating systems are better in terms of local air quality compared to heating systems installed in both newly built and old individually heated houses.

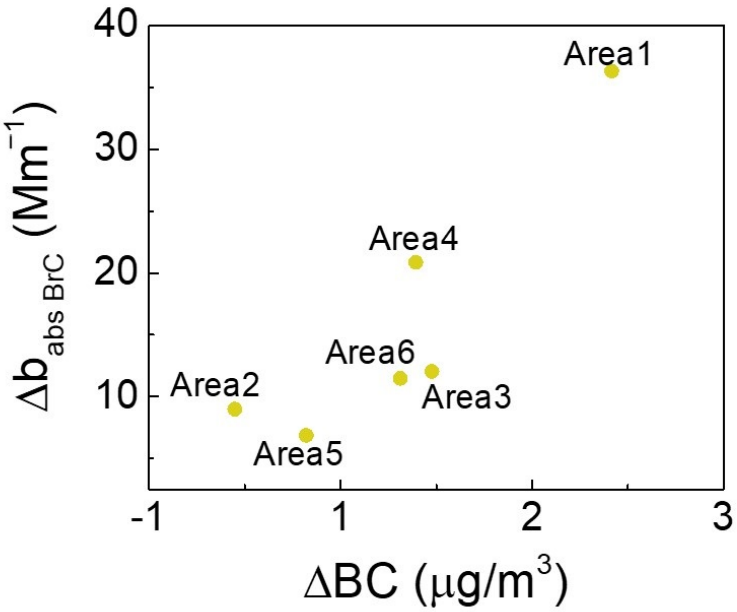

Figure 12. Difference in $b_{abs\ BrC}$ and BC between each area and the background station.

4. Conclusions

Carbonaceous particles were assessed in several characteristic city areas, along with the background station, in order to understand the importance of residential heating to local air quality. Analysis at the background station revealed that during the heating season, the mass concentration of biomass-burning-related organic aerosol factors (BBOA1 and BBOA2) and biomass-burning-related BC_{BB} were, respectively, 32% and 4% of the total PM_1. Both BBOA1 and BBOA2 showed significant mass absorption cross-section values (1.41 m^2g^{-1} and 2.63 m^2g^{-1} at 370 nm, respectively) and dominated the composition of BrC (33% and 62%, respectively). In addition, BrC accounted for 29% of the light absorption coefficient b_{abs} at 370 nm. These results were compared with those from six locations characterized by different predominant heating systems. It was found that in all urban areas, the input of BrC to the total b_{abs} was higher and varied between 33% and 70%. Additionally, it was observed that due to the highest difference between local and background station levels of BrC and BC, the worst air quality was in areas mainly or partly characterized by old wooden houses with outdated heating systems (solid fuel ovens, usually without installed exhaust filters). In those areas, BC levels were up to three times higher and b_{abs} attributed to BrC and BC_{BB} were, respectively, 4.6 and 4.4 times higher than at the background station.

Supplementary Materials: The following supporting information can be downloaded at: https://www.mdpi.com/article/10.3390/atmos14071054/s1, Figure S1: Pollution roses.

Author Contributions: Conceptualization, J.P.; methodology, J.P.; validation, J.P.; formal analysis, J.P.; investigation, J.P.; data curation, J.P. and V.D.; writing—original draft preparation, J.P.; writing—review and editing, J.P. and S.B.; visualization, J.P.; supervision, S.B.; project administration, J.P. and S.B. All authors have read and agreed to the published version of the manuscript.

Funding: This project received funding from the European Social Fund (project no. 09.3.3-LMT-K-712-23-0176) under a grant agreement with the Research Council of Lithuania (LMTLT).

Institutional Review Board Statement: Not applicable.

Informed Consent Statement: Not applicable.

Data Availability Statement: The data presented in this study are available on request from the corresponding author.

Conflicts of Interest: The authors declare no conflict of interest.

References

1. Carvalho, H. Air pollution-related deaths in Europe-time for action. *J. Glob. Health* **2019**, *9*, 2–5. [CrossRef]
2. Khomenko, S.; Cirach, M.; Pereira-Barboza, E.; Mueller, N.; Barrera-Gómez, J.; Rojas-Rueda, D.; de Hoogh, K.; Hoek, G.; Nieuwenhuijsen, M. Premature mortality due to air pollution in European cities: A health impact assessment. *Lancet Planet. Health* **2021**, *5*, e121–e134. [CrossRef] [PubMed]
3. Tobler, A.K.; Skiba, A.; Canonaco, F.; Močnik, G.; Rai, P.; Chen, G.; Bartyzel, J.; Zimnoch, M.; Styszko, K.; Nęcki, J.; et al. Characterization of non-refractory (NR) PM1 and source apportionment of organic aerosol in Kraków, Poland. *Atmos. Chem. Phys.* **2021**, *21*, 14893–14906. [CrossRef]
4. Juda-Rezler, K.; Reizer, M.; Maciejewska, K.; Błaszczak, B.; Klejnowski, K. Characterization of atmospheric $PM_{2.5}$ sources at a Central European urban background site. *Sci. Total Environ.* **2020**, *713*, 136729. [CrossRef]
5. Yang, Y.; Lou, S.; Wang, H.; Wang, P.; Liao, H. Trends and source apportionment of aerosols in Europe during 1980–2018. *Atmos. Chem. Phys.* **2020**, *20*, 2579–2590. [CrossRef]
6. van der Zee, S.C.; Fischer, P.H.; Hoek, G. Air pollution in perspective: Health risks of air pollution expressed in equivalent numbers of passively smoked cigarettes. *Environ. Res.* **2016**, *148*, 475–483. [CrossRef]
7. Lin, W.; Dai, J.; Liu, R.; Zhai, Y.; Yue, D.; Hu, Q. Integrated assessment of health risk and climate effects of black carbon in the Pearl River Delta region, China. *Environ. Res.* **2019**, *176*, 108522. [CrossRef]
8. Li, Y.; Henze, D.K.; Jack, D.; Henderson, B.H.; Kinney, P.L. Assessing public health burden associated with exposure to ambient black carbon in the United States. *Sci. Total Environ.* **2016**, *539*, 515–525. [CrossRef]
9. Paglione, M.; Gilardoni, S.; Rinaldi, M.; Decesari, S.; Zanca, N.; Sandrini, S.; Giulianelli, L.; Bacco, D.; Ferrari, S.; Poluzzi, V.; et al. The impact of biomass burning and aqueous-phase processing on air quality: A multi-year source apportionment study in the Po Valley, Italy. *Atmos. Chem. Phys.* **2020**, *20*, 1233–1254. [CrossRef]
10. Liakakou, E.; Kaskaoutis, D.G.; Grivas, G.; Stavroulas, I.; Tsagkaraki, M.; Paraskevopoulou, D.; Bougiatioti, A.; Dumka, U.C.; Gerasopoulos, E.; Mihalopoulos, N. Long-term brown carbon spectral characteristics in a Mediterranean city (Athens). *Sci. Total Environ.* **2020**, *708*, 135019. [CrossRef] [PubMed]
11. Cordell, R.L.; Mazet, M.; Dechoux, C.; Hama, S.M.L.; Staelens, J.; Hofman, J.; Stroobants, C.; Roekens, E.; Kos, G.P.A.; Weijers, E.P.; et al. Evaluation of biomass burning across North West Europe and its impact on air quality. *Atmos. Environ.* **2016**, *141*, 276–286. [CrossRef]
12. Becerril-Valle, M.; Coz, E.; Prévôt, A.S.H.; Močnik, G.; Pandis, S.N.; Sánchez de la Campa, A.M.; Alastuey, A.; Díaz, E.; Pérez, R.M.; Artíñano, B. Characterization of atmospheric black carbon and co-pollutants in urban and rural areas of Spain. *Atmos. Environ.* **2017**, *169*, 36–53. [CrossRef]
13. Crippa, M.; Canonaco, F.; Lanz, V.A.; Äijälä, M.; Allan, J.D.; Carbone, S.; Capes, G.; Ceburnis, D.; Dall'Osto, M.; Day, D.A.; et al. Organic aerosol components derived from 25 AMS data sets across Europe using a consistent ME-2 based source apportionment approach. *Atmos. Chem. Phys.* **2014**, *14*, 6159–6176. [CrossRef]
14. Daellenbach, K.R.; Stefenelli, G.; Bozzetti, C.; Vlachou, A.; Fermo, P.; Gonzalez, R.; Piazzalunga, A.; Colombi, C.; Canonaco, F.; Hueglin, C.; et al. Long-term chemical analysis and organic aerosol source apportionment at nine sites in central Europe: Source identification and uncertainty assessment. *Atmos. Chem. Phys.* **2017**, *17*, 13265–13282. [CrossRef]
15. Bertrand, A.; Stefenelli, G.; Bruns, E.A.; Pieber, S.M.; Temime-Roussel, B.; Slowik, J.G.; Prévôt, A.S.H.; Wortham, H.; El Haddad, I.; Marchand, N. Primary emissions and secondary aerosol production potential from woodstoves for residential heating: Influence of the stove technology and combustion efficiency. *Atmos. Environ.* **2017**, *169*, 65–79. [CrossRef]
16. Bond, T.C.; Streets, D.G.; Yarber, K.F.; Nelson, S.M.; Woo, J.H.; Klimont, Z. A technology-based global inventory of black and organic carbon emissions from combustion. *J. Geophys. Res. D Atmos.* **2004**, *109*, 1–43. [CrossRef]
17. Meyer, N.K. Particulate, black carbon and organic emissions from small-scale residential wood combustion appliances in Switzerland. *Biomass Bioenergy* **2012**, *36*, 31–42. [CrossRef]
18. Blanco-Donado, E.P.; Schneider, I.L.; Artaxo, P.; Lozano-Osorio, J.; Portz, L.; Oliveira, M.L.S. Source identification and global implications of black carbon. *Geosci. Front.* **2022**, *13*, 101149. [CrossRef]
19. Nie, D.; Qiu, Z.; Wang, X.; Liu, Z. Characterizing the source apportionment of black carbon and ultrafine particles near urban roads in Xi'an, China. *Environ. Res.* **2022**, *215*, 114209. [CrossRef]
20. Adler, G.; Wagner, N.L.; Lamb, K.D.; Manfred, K.M.; Schwarz, J.P.; Franchin, A.; Middlebrook, A.M.; Washenfelder, R.A.; Womack, C.C.; Yokelson, R.J.; et al. Evidence in biomass burning smoke for a light-absorbing aerosol with properties intermediate between brown and black carbon. *Aerosol Sci. Technol.* **2019**, *53*, 976–989. [CrossRef]
21. Kirchstetter, T.W.; Thatcher, T.L. Contribution of organic carbon to wood smoke particulate matter absorption of solar radiation. *Atmos. Chem. Phys.* **2012**, *12*, 6067–6072. [CrossRef]
22. Gao, P.; Zhou, C.; Lian, C.; Wang, X.; Wang, W. Morphology and Composition of Insoluble Brown Carbon from Biomass Burning. *ACS Earth Space Chem.* **2022**, *6*, 1574–1580. [CrossRef]
23. Drinovec, L.; Močnik, G.; Zotter, P.; Prévôt, A.S.H.; Ruckstuhl, C.; Coz, E.; Rupakheti, M.; Sciare, J.; Müller, T.; Wiedensohler, A.; et al. The "dual-spot" Aethalometer: An improved measurement of aerosol black carbon with real-time loading compensation. *Atmos. Meas. Tech.* **2015**, *8*, 1965–1979. [CrossRef]
24. Sandradewi, J.; Prévôt, A.S.H.; Weingartner, E.; Schmidhauser, R.; Gysel, M.; Baltensperger, U. A study of wood burning and traffic aerosols in an Alpine valley using a multi-wavelength Aethalometer. *Atmos. Environ.* **2008**, *42*, 101–112. [CrossRef]

25. Zotter, P.; Herich, H.; Gysel, M.; El-Haddad, I.; Zhang, Y.; Močnik, G.; Hüglin, C.; Baltensperger, U.; Szidat, S.; Prévôt, A.S.H. Evaluation of the absorption Ångström exponents for traffic and wood burning in the Aethalometer-based source apportionment using radiocarbon measurements of ambient aerosol. *Atmos. Chem. Phys.* **2017**, *17*, 4229–4249. [CrossRef]
26. Qin, Y.M.; Bo Tan, H.; Li, Y.J.; Jie Li, Z.; Schurman, M.I.; Liu, L.; Wu, C.; Chan, C.K. Chemical characteristics of brown carbon in atmospheric particles at a suburban site near Guangzhou, China. *Atmos. Chem. Phys.* **2018**, *18*, 16409–16418. [CrossRef]
27. Middlebrook, A.M.; Bahreini, R.; Jimenez, J.L.; Canagaratna, M.R. Evaluation of Composition-Dependent Collection Efficiencies for the Aerodyne Aerosol Mass Spectrometer using Field Data. *Aerosol Sci. Technol.* **2012**, *46*, 258–271. [CrossRef]
28. Paatero, P. A weighted non-negative least squares algorithm for three-way "PARAFAC" factor analysis. *Chemom. Intell. Lab. Syst.* **1997**, *38*, 223–242. [CrossRef]
29. Weimer, S.; Alfarra, M.R.; Schreiber, D.; Mohr, M.; Prévôt, A.S.H.; Baltensperger, U. Organic aerosol mass spectral signatures from wood-burning emissions: Influence of burning conditions and wood type. *J. Geophys. Res.* **2008**, *113*, D10304. [CrossRef]
30. Pauraite, J.; Minderytė, A.; Dudoitis, V.; Plauškaitė, K.; Byčenkienė, S. Effect of urban submicron particles on single scattering albedo: The case study of high pollution event. *J. Quant. Spectrosc. Radiat. Transf.* **2022**, *280*, 108075. [CrossRef]
31. Pauraite, J.; Plauškaitė, K.; Dudoitis, V.; Ulevicius, V. Relationship between the Optical Properties and Chemical Composition of Urban Aerosol Particles in Lithuania. *Adv. Meteorol.* **2018**, *2018*, 8674173. [CrossRef]
32. Minderytė, A.; Pauraite, J.; Dudoitis, V.; Plauškaitė, K.; Kilikevičius, A.; Matijošius, J.; Rimkus, A.; Kilikevičienė, K.; Vainorius, D.; Byčenkienė, S. Carbonaceous aerosol source apportionment and assessment of transport-related pollution. *Atmos. Environ.* **2022**, *279*, 119043. [CrossRef]
33. Ng, N.L.; Canagaratna, M.R.; Zhang, Q.; Jimenez, J.L.; Tian, J.; Ulbrich, I.M.; Kroll, J.H.; Docherty, K.S.; Chhabra, P.S.; Bahreini, R.; et al. Organic aerosol components observed in Northern Hemispheric datasets from Aerosol Mass Spectrometry. *Atmos. Chem. Phys.* **2010**, *10*, 4625–4641. [CrossRef]